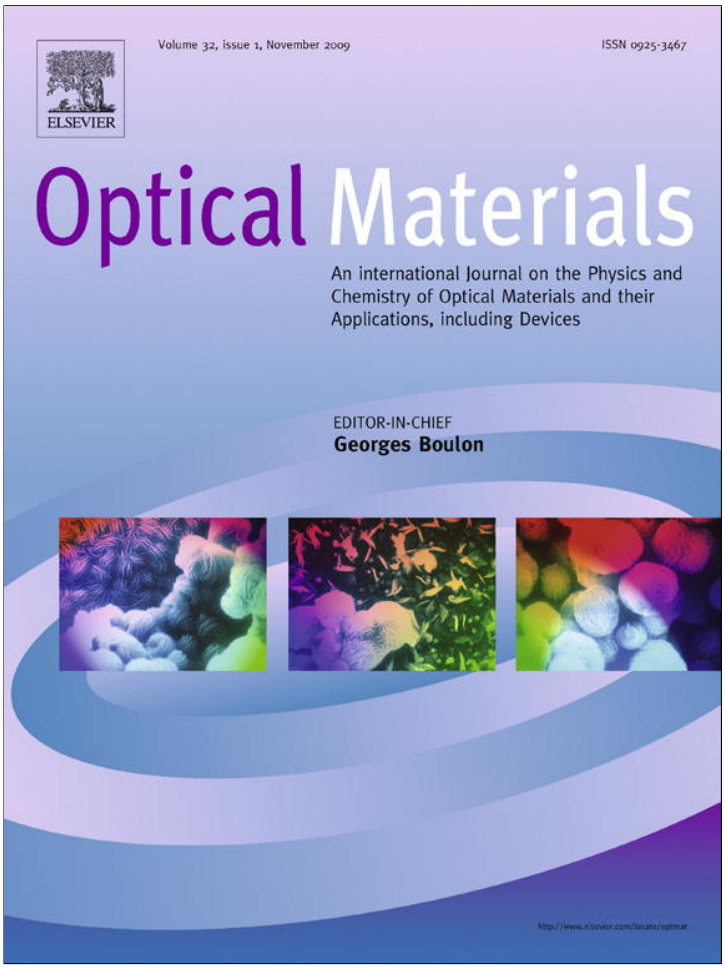

Optical Materials 32 (2009) 62–68

Contents lists available at ScienceDirect

Optical Materials

journal homepage: www.elsevier.com/locate/optmat

Optical properties of transparent nanocrystalline yttria stabilized zirconia

J.E. Alaniz, F.G. Perez-Gutierrez, G. Aguilar, J.E. Garay *

Department of Mechanical Engineering, Materials Science and Engineering Program, University of California, Riverside, CA 92521, United States

ARTICLE INFO

Article history:
Received 10 December 2008
Received in revised form 21 May 2009
Accepted 15 June 2009
Available online 16 July 2009

Keywords:
Nanocrystalline ceramics
Grain boundaries
Transparent ceramics
Spark plasma sintering

ABSTRACT

The optical properties of transparent nanocrystalline zirconia produced using a current activated method were characterized over the entire visible spectrum. The resolutions of the samples were characterized using standard resolution targets. All of the samples produced were found to have as high a resolution as detectable from the test, i.e., they are transparent not translucent. Transmission, reflectance, and absorption coefficients are reported for various wavelengths. The absorption coefficients were found to be highly dependent on processing time. Annealing experiments helped determine that oxygen vacancies (with free electrons) are the primary absorption centers in the visible wavelengths. In addition it was found that grain boundary cores or their associated defects do not contribute significantly to light absorption in the visible range. The lack of an influence of the grain boundary regions is discussed in terms of low oxygen vacancy concentration in the grain boundary space charge layer.

1. Introduction

Recently there has been increasing interest in transparent ceramics spurred by wide ranging applications such as high temperature window/viewports, optical electronics, and transparent armor. Transparent Al_2O_3 (alumina), $MgAl_2O_4$ (spinel), indium tin oxide (ITO), and $Y_3Al_5O_{12}$ (yttrium aluminum garnet or YAG) have been the most studied systems. Since polycrystalline yttria stabilized zirconia (YSZ) is one of the most versatile engineering ceramics, introduction of optical transparency to this ceramic should yield an exceptionally versatile material. Well documented properties of YSZ are high hardness, toughness, and high oxygen diffusivity. In addition, low thermal conductivity makes it an excellent thermal barrier material. However, this material has traditionally been opaque with a white to grayish appearance in its polycrystalline form.

The promise of excellent multifunctionality has promoted work in harnessing the light transmittance properties of polycrystalline YSZ. Recently the elusive goal of producing optically transparent polycrystalline YSZ has been attained by two groups both using spark plasma sintering (SPS) [1,2]. Anselmi-Tamburini et al. [1] used a high pressure version of the SPS (~480 MPa), while Casolco et al. used a traditional die set up and two-step load application procedure [2]. Both groups produced large samples (10 mm [1] and 19 mm [2] diameters) with high degrees of transparency. In the latter case, the color of the samples was shown to change dramatically with processing conditions. Natural applications of these ceramics with high optical transparency coupled with very low thermal conductivity and good toughness are high temperature windows. They also have potential as varying color filters in extreme environments and impact/scratch resistant electronic displays.

Although the optical properties of single crystal YSZ are well documented [3,4], the inherent optical properties (reflectivity, absorption coefficient) of bulk nanocrystalline YSZ have not been reported. There has been a resurgence of interest in polycrystalline optical ceramics and hence on the effects of grain boundaries on optical properties. The role of grain boundaries on optical properties becomes crucial in nanocrystalline ceramics that have a significantly higher concentration of grain boundaries than their microcrystalline counterparts. Grain boundaries can be envisioned to change light transmission for various reasons. In solids with an anisotropic refractive index, grain boundaries could serve as scattering sites since they form the boundary between crystallites with different orientation. This effect is likely responsible for the increased light transmittance in fine grained alumina [6]. Another mechanism is the possible absorption by point defects associated with grain boundaries. This effect has not been widely discussed in the literature. YSZ is an ideal material for exploring the latter case since it has known grain boundary associated defects. In this article we present experimental data on the transmission, reflection, and the absorption coefficient in the visible range for nanocrystalline YSZ with varying colors in order to elucidate the role of grain boundary defects on optical properties.

Our samples were produced using spark plasma sintering (SPS). SPS is related to hot pressing in that the powder is heated while pressure is applied. However, in hot pressing, heating is accomplished externally by way of a heating coil while SPS uses a high density current flux through the sample and the die to cause Joule heating within the sample. This unique technique allows us to

* Corresponding author. Tel.: +1 951 827 2449.
E-mail address: jegaray@engr.ucr.edu (J.E. Garay).

0925-3467/$ - see front matter © 2009 Elsevier B.V. All rights reserved.
doi:10.1016/j.optmat.2009.06.004

decrease the heating time and the cooling time of the sintering process. This minimizes the amount of grain growth in the material and maintains the nanometric grains of the powder. A nanostructure in ceramics has a number of benefits. The mechanical properties (hardness and toughness) are sensitive to the concentration of grain boundaries within the sample. In fact nanocrystalline YSZ has perhaps the highest fracture toughness of any monolithic transparent ceramic reported [2]. Here we explore the consequences of nanocrystallinity on the optical properties of YSZ.

2. Experimental procedure

2.1. Sample preparation

Commercial (Tosoh Corporation, Tokyo, Japan) nanocrystalline 8YSZ powder with a reported grain size of 50 nm was densified using SPS. Each of the samples was prepared in a graphite die with 19 mm inner diameter. Temperature was measured using a grounded k type thermocouple placed in a hole drilled halfway through the thickness of the die. The sintering process was performed in a fabricated vacuum chamber ($<4 \times 10^{-4}$ Torr) with built in water cooling. The DC current used for sintering was provided by programmable power supplies (Xantrex Inc., Canada) while the pressure was delivered to the copper electrodes by an Instron universal test frame (Instron Inc., USA).

1.5 g of the powder was loaded into the die for each sample. The pressure in the system was raised to 106 MPa before the current was applied. Once this had been accomplished, the current heated the sample to 1200 °C, after which the pressure was steadily raised to 141 MPa. Samples were held for varying times at the final pressure and temperature (10, 11, and 12 min). Details of this two-step load procedure and its effects have been reported earlier [2]. The densified samples were fractured and examined using SEM (Phillips FEI). The grain size was measured by optical analysis on the resulting micrographs.

2.2. Optical characterization

To measure the optical properties of the YSZ (transmittance, reflectance, and absorption coefficient), a standard integrating sphere-laser experimental setup was used [5]. Slightly different arrangements were used to measure transmittance and reflectance, as illustrated in Fig. 1a and b, respectively. The photodiodes (PD1 and PD2) are located in positions given in the schematic (Fig. 1). While PD2 is used to measure either transmittance or reflectance on each of these arrangements, PD1 is placed next to a beam splitter to directly measure the incident light on the sample during the reflectance measurements. The beam splitter was removed for the transmission measurements, and the maximum power of the incident light was measured once.

With transmittance and reflectance measured, absorbance can be readily calculated. The laser light was provided by a Q-switched, Nd:YAG laser coupled to an Optical Parametric Oscillator (OPO), capable of emitting 6 ns laser pulses at 10 Hz at wavelengths from 355 to 2300 nm (EKSPLA, Lithuania). The wavelengths used for these experiments were 450, 497, 525, 543, 566, 588, 610, 633, and 800 nm. This work is focused on the optical properties of YSZ samples within the visible spectrum only, thus wavelengths longer than 800 nm were not considered.

2.2.1. Calibration

To calibrate the photodiodes (PD1 and PD2) shown in Fig. 1a and b, the average power emitted from the laser was measured with a standardized power meter (Ophir Optronics Solutions, Israel) and the voltage output of the two PDs were recorded for the different wavelengths and laser power used.

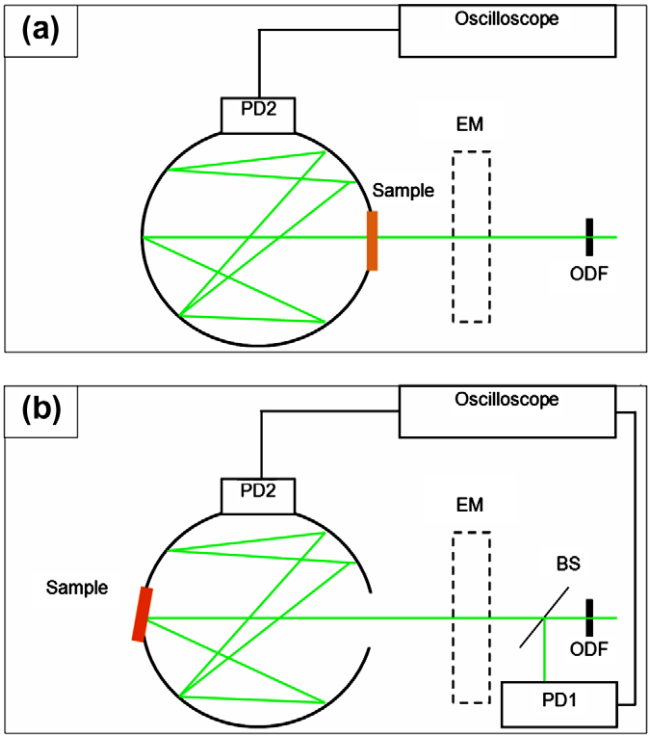

Fig. 1. Schematic of the (a) transmission and (b) reflection setups for the integrating spheres.

When the maximal laser power saturated the PDs, the incident light was attenuated with optical density filters (ODF) until the PDs output was within the manufacturer specified parameters (less than 2 V in this case). For these cases, the power of the light entering the sphere (P_{Sphere}) was computed using Eq. (1), where P_{Laser} is the maximal laser power and OD is the total optical density of the filters in the path of the beam. The PDs output voltage was displayed on an oscilloscope and recorded.

$$P_{\text{Sphere}} = \frac{P_{\text{Laser}}}{10^{\text{OD}}} \tag{1}$$

To calibrate the PDs over the whole range of power and wavelengths used for this study, a series of ODF's were placed in front of the sample in increments of 0.1 OD, thus decreasing the power incident on the PD for each wavelength. The variation of the PDs output signal with laser power (P_{Sphere}) showed an expected linear dependence which was represented by a best-fit line.

After calibration, the sample was mounted to the sample port on the sphere (front for transmittance, Fig. 1a; back for reflectance, Fig 1b). When necessary, ODFs were placed between the laser and the sample until the PDs output was maximized. With the sample in place, ten voltage measurements were taken with up to ten different ODF. For each filter, the equation of the best-fit line of the sensor calibration plot was used to calculate the power measured by PD2 (P_{Diode}).

2.2.2. Transmittance and reflectance

The transmittance coefficient is the ratio of light transmitted through the sample to the total light incident upon that sample. Since P_{Sphere} is equivalent to the total power transmitted through the sample (P_{Diode}), we can find the transmittance (T) of the sample using Eq. (2)

$$T = \frac{P_{\text{Diode}}}{P_{\text{Sphere}}} \tag{2}$$

After each sample was tested with ten different ODF, the average transmittance was taken for all ten readings and the percent error was calculated for each transmittance value. As one final test to make sure the calibration of the photodiode was correct, the sample was removed and a reading was taken with an ODF of 0.8 OD to verify that T was acceptably close to one hundred percent, as we would expect. The reflection of the sample is measured in a similar way, but due to the change in setup shown in Fig. 1, P_{Diode} is a measurement of the light reflected by the sample rather than a measurement of the light transmitted. Also, in the calibration step in which the sample is removed from the sphere, it was verified that the reflection was zero percent rather than one hundred.

2.2.3. Absorption

The absorption coefficient was calculated using the data from the transmittance and reflectance experiments and Beer's law, given by

$$T = (1 - R)^2 e^{-\beta l} \tag{3}$$

where l is the sample thickness, T is transmittance, R for reflectance, and β the absorption coefficient. Thus the absorption coefficient is given by

$$\beta = \frac{2\ln(1 - R) - \ln T}{1} \tag{4}$$

The absorption coefficient was calculated using Eq. (4) for each of the wavelengths measured.

2.2.4. Resolution

In order to establish the transparency of our samples, we used a National Bureau of Standards NBS 1963A resolution target. This resolution target is commonly used for comparing optical lenses and can serve as a standard for establishing adequate resolution for optical applications. Through a microscope, it is possible to determine what the minimum optical resolution of the sample is through a range of 18–1 cycle/mm. A digital camera was used to take photographs. One cycle is an entire dark line and an entire light line; i.e., one black line is 27.8 μm wide on the 18 cycles/mm grating.

2.2.5. Annealing experiments (reoxidation)

In order to characterize the effect of annealing on the optical properties of densified YSZ, a sample was annealed in a furnace at 750 °C. Before annealing, the transmittance and reflectance of the sample was taken. After the sample had been annealed 2, 4, 8, 16, and 24 h, these data were taken again for comparison. All measurements were taken using light with 633 nm wavelength. This provides a study of the change in optical characteristics as the oxygen content changes within the bulk material.

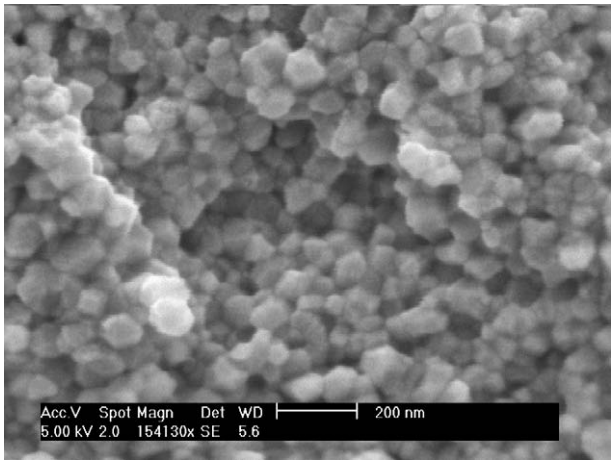

Fig. 2. SEM micrograph of a fracture surface of YSZ sample processed at 1200 °C and held for 10 min. This microstructure is representative of all samples in this work having an average grain size is 55 nm.

3. Results

Density measurements show that the 8YSZ samples, processed for 10, 11, and 12 min are fully densified (+99.9%). A representative micrograph of a fracture surface is shown in Fig. 2. Image analysis on many such micrographs showed that the YSZ samples have average grain sizes of 55 nm.

Although they all transmit light they are visibly different colors (getting progressively darker with hold time). The 10 min sample is an amber brown color, the 11 min sample is dark orange, and the 12 min sample is a ruby-red color when transmitted light is observed through them. Fig. 3 shows results typical of the NBS reso-

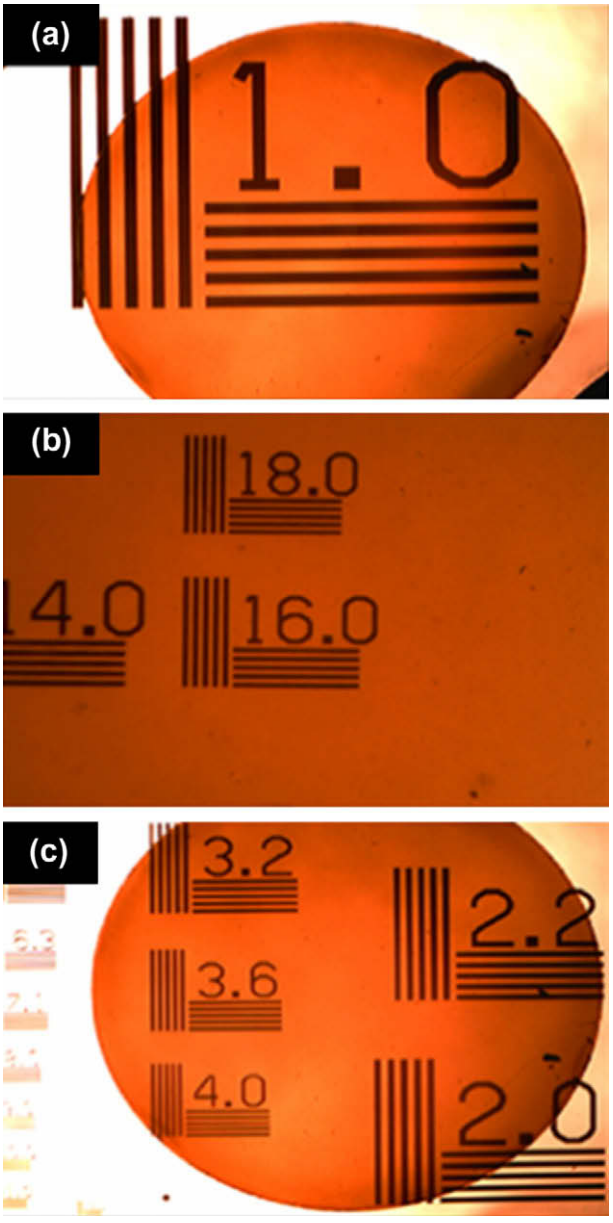

Fig. 3. Photographs of the NBS 1963A resolution target through the reoxidation sample after 2 h of annealing. The resolutions shown are the (a) 1 cycle/mm target (Each black line is .5 mm) and the (b) 18 cycle/mm target (Each black line is 27.78 μm). A photograph of the sample covering a wide variety of resolutions (c) shows that the sample does not alter the transmitted image at all.

lution tests. Fig. 3a–c are pictures that demonstrate the high optical resolution of our samples at increasingly high magnifications. All of our samples, including the re-oxidized samples clearly show the highest resolution (18 cycles/mm) on the resolution target as shown in Fig. 3b.

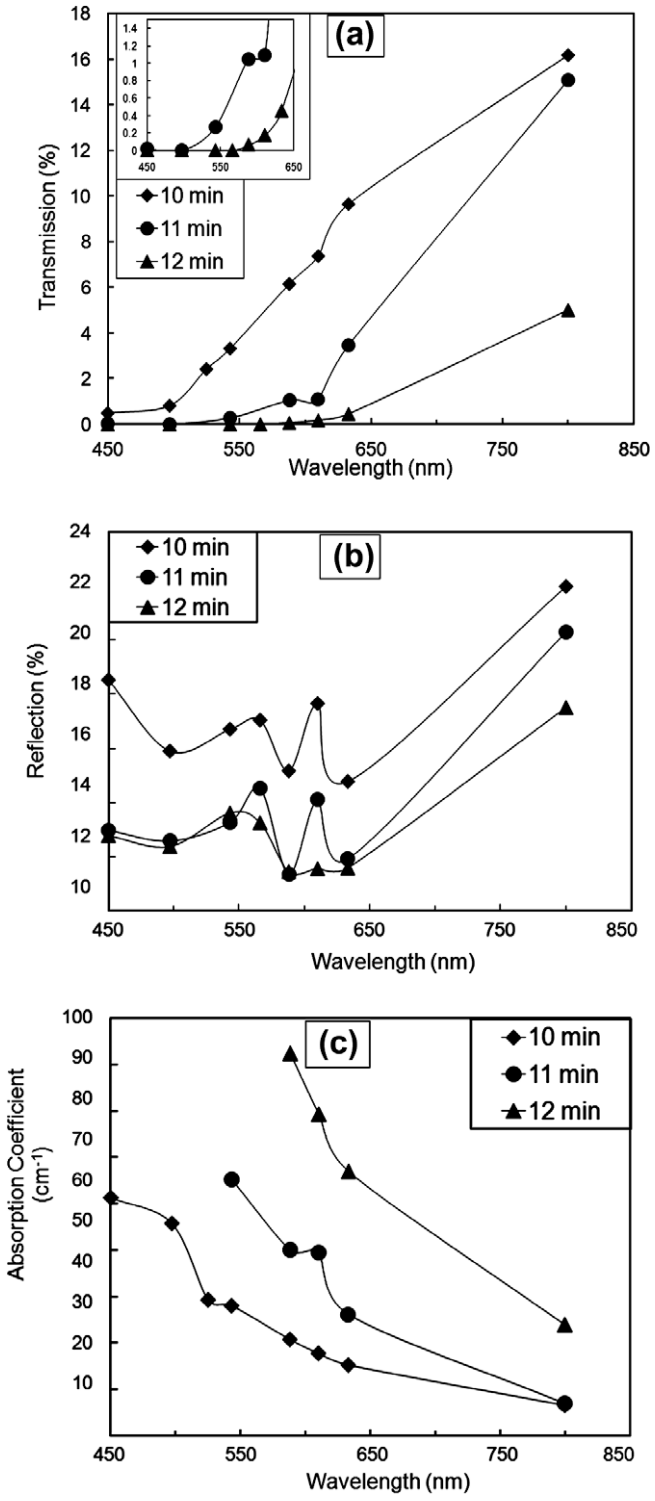

Fig. 4. Transmission (a), reflection (b), and absorption (calculated) (c) coefficients for YSZ samples processed with varying hold times (10, 11, and 12 min) for wavelengths throughout the visible spectrum. The inset in 3a contains an enlarged portion of the graph that focuses in on the low transmission behavior of the sample that was held at processing temperature for 12 min.

Fig. 4a shows the transmission measurements of the three samples that were processed using 10, 11, and 12 min holds. The transmission decreases greatly for any given wavelength as the process holding time is increased. In addition, the samples appear to transmit a higher percentage of light as the wavelength of the incident light is increased. All of the transmission measurements taken for each of the wavelengths were within ten percent of the value shown, which is approximately the same size as the marker shown or smaller.

The reflection of the 10, 11, and 12 min samples is shown in Fig. 4b. It can be seen that the reflection curves for all three samples are approximately the same shape. Also, while the reflection of the 11 and 12 min samples is approximately the same, the 10 min sample is noticeably higher. All of the reflection measurements taken for each of the wavelengths were within ten percent of the value shown, which is approximately the same size as the marker shown or smaller.

The absorption data shown in Fig. 4c is an intrinsic material property calculated using the reflection and transmission data and Eq. (2). It can be seen that as the incident light is increased in wavelength, the absorption of the sample decreases dramatically. Also, the absorption of the stabilized zirconia increases quite a bit as the sintering time is increased.

There are striking qualitative differences in the appearance of the re-oxidized sample as the annealing time increased. The sample was a dark red color when it was first removed from the sintering device, but as it was annealed, it gradually became a lighter milky white color. Fig. 5a shows that as the annealing time of the sample is increased, the transmission of the sample also increases. After just twenty four hours of annealing, the transmission of our sample increased by a factor of ten. Fig. 5b shows that the reflection also increases to a large degree as the sintering time is increased. In comparison, the absorption coefficient of YSZ (Fig. 5c) appears to decrease quite rapidly as the material is annealed. All of these measurements were taken with red light with a wavelength of 633 nm. All of the measurements for each of these characteristics were within ten percent of the value shown which is denoted by the size of the marker itself. Furthermore, after each annealing period, the resolution target tests were performed using the procedure described above. Each time, it was noted that the samples clearly resolved a grating of 18 cycles/mm.

For convenient comparison, the wavelength dependent properties of the as-processed 10 min sample and the 10 min sample annealed for 24 h are plotted in Figs. 6 and 7. When the transmission of the annealed sample is directly compared to that of the as-processed sample (Fig. 6), it is clear that throughout the visible spectrum the annealed sample transmits much more light. Likewise, Fig. 7 shows that the absorption coefficient of the annealed sample is much smaller than that of the as-processed sample. Also plotted in Fig. 7 are previously reported single crystal YSZ absorption coefficients from Savioni et al. [4]. Comparison reveals that the wavelength dependent absorption coefficients are qualitatively and quantitatively similar for our samples and single crystals in both the reduced and non-reduced states.

4. Discussion

Light incident upon our nanocrystalline samples can be reflected, scattered, or absorbed within the bulk. Previous work on ceramics densified from powders has confirmed that scattering is the primary reason for the opacity of most ceramics. In turn it has been found that light scattering is largely a function of the porosity of a material. Apetz et al. showed that the absorption of transparent alumina depends on the porosity and pore size of a sample [6]. Anselmi-Tamburini et al. also found that density

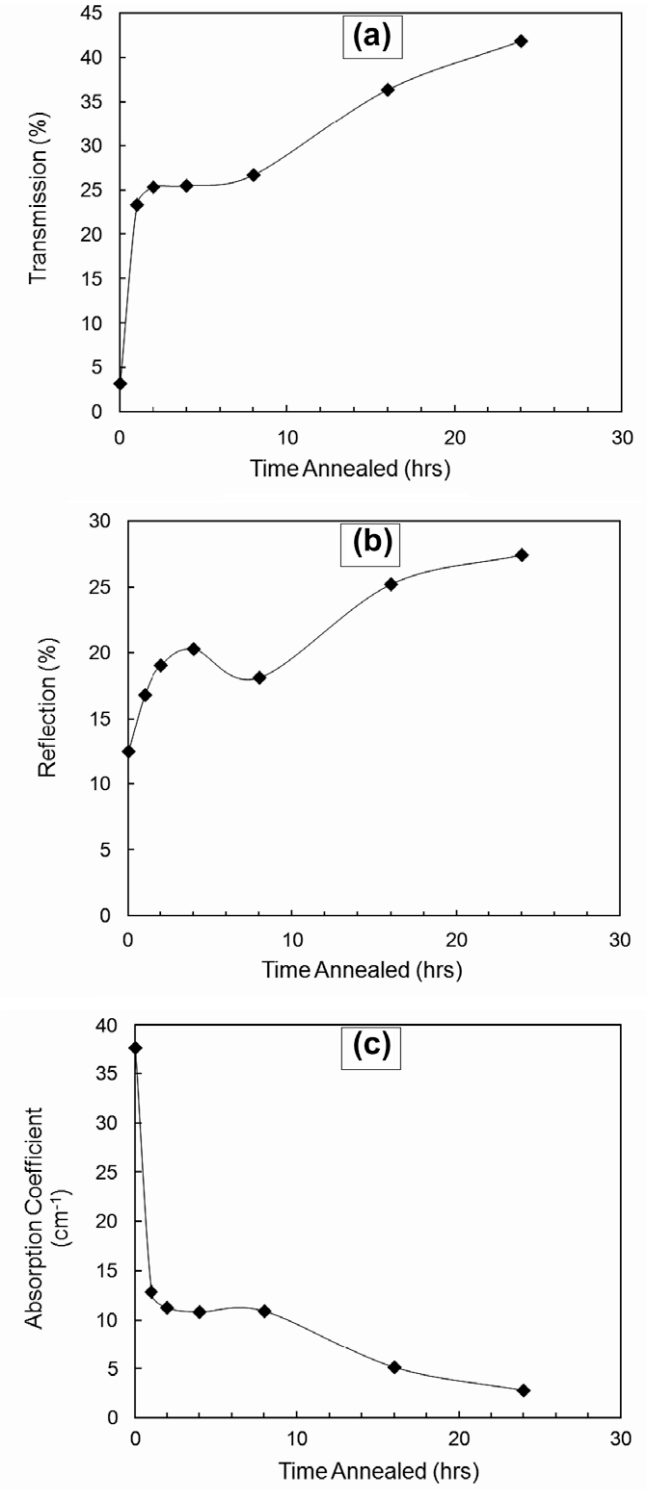

Fig. 5. Transmission (a), reflection (b), and absorption coefficients (c) vs. annealing time for a sample produced using a 10 min hold. All data was taken using 633 nm light. The annealing was done at 750 °C in air.

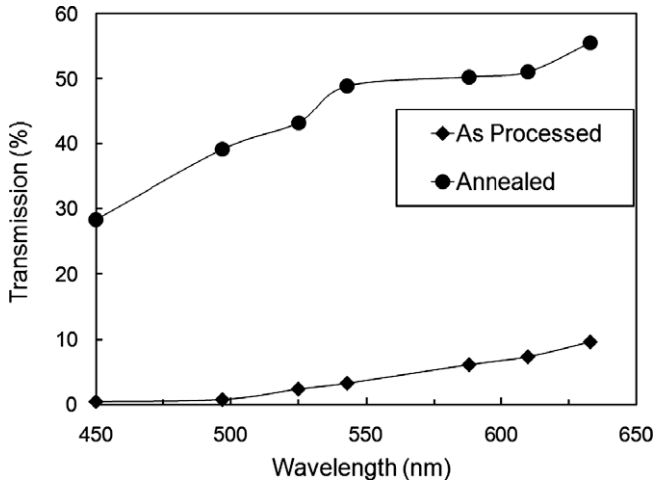

Fig. 6. Comparison of transmission measurements of as-produced and re-oxidized samples. Both samples were produced using the same procedure (10 min hold time). The re-oxidized sample was annealed at 750 °C for over 24 h.

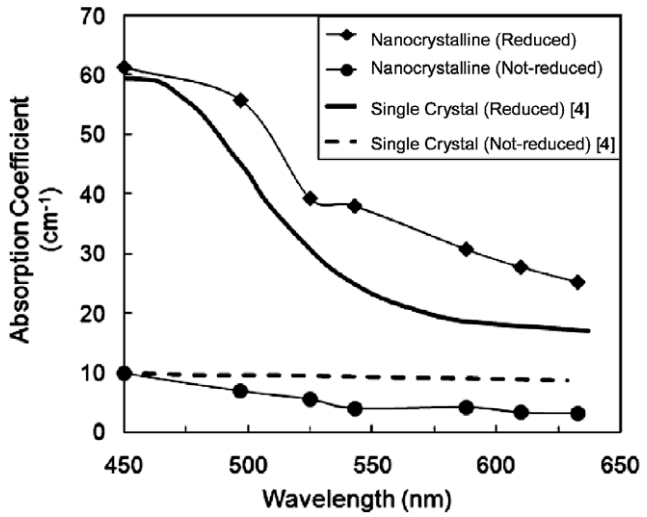

Fig. 7. Comparison of the absorption coefficient of as-produced (reduced) and re-oxidized (not-reduced) samples. Both samples were produced using the same procedure (10 min hold time). The annealed sample was annealed at 750 °C for over 24 h. Also plotted are results from previous work [4] on reduced and not-reduced single crystal YSZ. The similarity of the single crystal and nanocrystalline samples suggest that grain boundaries do not play a major role in the optical properties in YSZ.

(porosity) plays a large role in the transparency of YSZ [1]. However, we do not believe that pore scattering plays a major role in the present work because our samples are all 99.9% dense and have very small grain sizes. At such low levels of porosity, Anselmi-Tamburini et al. [1], calculated that only pores larger than ~50 nm cause significant scattering and thus reduction of transmission. We do not believe such large pores can exist in our samples. This is because in samples densified from nanometric powders using mechanical pressure, it is highly unlikely that the pore diameter would be larger than the grain size (in high density materials). In fact pore diameter is usually significantly smaller than the average grain size which in this case is 55 nm.

More direct evidence that the porosity does not play a major role in the optical behavior comes from our annealing experiments (Fig. 5). Annealing the samples in air at 750 °C dramatically increases the transmission of our samples (Fig. 5a). At this temperature we expect exceedingly low cation mobility, so annealing has no effect on the porosity of the samples. If the reduced transmission was related to porosity, we would not expect annealing to have such a dramatic effect on the optical behavior. This conclusion is further supported by the high resolution that our samples have been shown to have (Fig. 3). Significant scattering would cause a resolution limit, which is not the case in our samples. Thus

we can assume that scattering can be safely neglected. In this light we will discuss our observations considering only absorption.

Examination of Fig. 4a reveals that the sample processed for 10 min transmits light at all of the wavelengths measured, but less light at lower wavelengths, making it appear yellowish-amber. The sample processed at 12 min transmits light significantly only at the red end of the spectrum and has a high absorption coefficient at the blue end (Fig. 4c), explaining its ruby-red appearance. The 11 min sample lies in the middle and is orange.

Investigations of reduced YSZ single crystals have reported several characteristic absorption bands [4]. The most prominent is centered at 470 nm (2.64 eV). In addition there are two others at 375 and 700 nm. Consistent with results on single crystals, the wavelength dependence of the absorption coefficient (Fig. 4c) of our nanocrystalline YSZ is dominated by the 470 nm absorption band. This is especially obvious in the 10 min sample, where we observe a clear shoulder. The absorption coefficients at this wavelength for the 11 and 12 min samples could not be reliably measured since the transmitted light was near zero. It is worth emphasizing that the 11 and 12 min samples are still transparent to higher wavelength light and the resolution is high as well. The decrease in transmission (Fig. 4a) and increase in absorption coefficient (Fig. 3c) can be attributed to absorption by the defect associated with the 470 nm band. We speculate that the 11 and 12 min samples have a higher concentration of this absorption center.

The question now arises as to what absorption center is responsible for the 470 nm absorption band. Previous studies on YSZ (single crystals) have attributed changes in absorption coefficient to point defects and/or colloidal metal formation due to either thermal or electrochemical reduction. A further possibility for absorption centers arises in our polycrystalline materials – absorption at grain boundaries (or grain boundary related defects).

Our processing method is conducive to both temperature and electrical current induced defect formation, because the SPS process uses a high density current flux and operates at relatively high temperatures. Wright et al. propose that colloidal metal (zirconium agglomerates form in heavily reduced single crystal zirconia [3] causing darkening and eventual opacity. Large metal agglomerates in our samples can be excluded for similar reasons to large pores; we do not observe a loss of optical resolution, which we would expect if we had any large agglomerates of metal in our sample. A much more likely case is that the 470 nm band is attributable to point defects as previously reported in single crystals [4]. The vacuum in combination with the graphite die at high temperatures of the densification process creates a highly reducing atmosphere leading to oxygen vacancies in the yttria stabilized zirconia. We believe that the dominant absorption centers in our nanocrystalline samples are oxygen vacancies associated with a free electron which can be written in the form:

$$V_O^{\cdot\cdot} + e' \rightarrow V_O \tag{5}$$

The dependence of optical properties on oxygen vacancy concentration is further supported by the annealing experiments. Annealing the YSZ samples in air should have the effect of diffusing oxygen back into the sample and removing the oxygen vacancies that were created at high temperatures. This process can also be seen as an annealing out of non-equilibrium oxygen vacancies. Thus if the transmission of light through a sample is related to the average concentration of oxygen vacancies then it should increase with time. In fact, Fig. 5a shows the remarkable increase in transmission when the samples are annealed for various times. Figs. 6 and 7 highlight the dramatic effect that annealing has on the transmission and absorption coefficients.

Comparison with previous absorption coefficients measured on single crystals (Fig. 7) shows a remarkable resemblance to the measurements of nanocrystalline YSZ in this work. Savoini et al. [4] measured the absorption coefficient for as grown single crystals and thermochemically reduced crystals. Qualitatively, both the reduced and non-reduced samples show similar behavior to our samples. The small difference in absorption values can be attributed to differences in absorption center concentrations (oxygen vacancies with free electrons). In other words the absorption coefficients of nanocrystalline samples with high and low oxygen vacancy concentrations are similar to their single crystal analogs. The similarity of the absorption properties of our nanocrystalline samples to single crystal results strongly suggests that grain boundaries (or their associated defects) do not intrinsically affect the optical properties of YSZ.

It is not surprising that grain boundaries are not a significant source of scattering in our samples since both the grain boundary width (~1 nm) and grain diameter (55 nm) are significantly smaller than the wavelength of light in the transparent range. In addition YSZ has an isotropic refractive index so the grain boundaries are not expected to behave as refractive interfaces separating grains with dissimilar orientations. However, the lack of absorption at grain boundaries is not as intuitive. We believe the lack of absorption by grain boundaries (or their associated defects) is due to the inherently low oxygen vacancy concentrations in the grain boundary region as explained below.

In general grain boundaries are known to have more open structure than perfect crystal regions [7,8]. Further complications arise in ionic crystals like YSZ due to ordering and charge balance considerations. The structures of grain boundaries in YSZ have been studied experimentally and theoretically [9–11]. Shibata et al. [11] examined a wide variety of grain boundary structures using high resolution transmission electron microscopy (HRTEM). For all $\Sigma = n$ (using coincident site lattice notation) they found a prevalence of Zr ions at the grain boundary core. Guo performed grain boundary enrichments studies using different ions with different valences. He found that di- and trivalent impurities enrich YSZ grain boundaries while tetra- and pentavalent impurities do not [9,10]. These studies have established that grain boundary cores are composed primarily of cations and are therefore positively charged. Zr or Y ions alone are not expected to significantly alter light absorption since they are colorless. Thus grain boundary *cores* are not expected to serve as absorption sites. However, there are other defects associated with grain boundaries as discussed below.

To retain charge neutrality, a negatively charged space charge layer (SCL) develops on either side of the positively charged grain boundary core. Since oxygen vacancies ($V_O^{\cdot\cdot}$) are positively charged, the space charge layer has a low oxygen vacancy concentration and should have a high yttrium ion concentration since yttrium ions on the Zr sublattice (Y'_{Zr}) are negatively charged. Indeed a low concentration of oxygen vacancies ($V_O^{\cdot\cdot}$) and high concentration of yttrium (Y'_{Zr}) has been found in the SCL [9,10]. The low oxygen vacancy concentration in the space charge layer would preclude the grain boundaries from having much of an effect on the absorption coefficient, since oxygen vacancies are the primary absorption centers as discussed above. Moreover we conclude that the cation rich grain boundary cores or the yttrium antisites (Y'_{Zr}) present in the SCL do not play a significant role in the absorption of light in the visible range.

5. Conclusion

Optical characterization of dense nanocrystalline YSZ made by SPS revealed that the absorption coefficient and light transmission can be readily altered using processing time. In addition these properties can be tailored by post-processing annealing in air. All of the samples had high resolution as confirmed by NBS 1963A resolution targets. Absorption in the visible range was attributed pri-

marily to oxygen vacancies associated with a free electron. Similarities of the absorption coefficient to single crystal suggest that grain boundary or grain boundary associated defects do not significantly alter the optical properties in the visible range. This finding can be rationalized by the low concentration of oxygen vacancies near grain boundaries (in SCL). The lack of absorption at grain boundaries is important for the development of nanocrystalline ceramics that have very high concentration of grain boundaries. These findings could be technologically significant because nanocrystallinity has been previously shown to improve the mechanical properties [2]. Good (and highly tailorable) optical properties coupled with good mechanical properties makes nanocrystalline YSZ an attractive material for a variety of applications.

Acknowledgements

Support from the Army Research Office through a Young Investigator Program (ARO-YIP) with William M. Mullins as Program Manager is most gratefully acknowledged. The authors would also like to thank G. Dominguez for help with sample preparation.

References

[1] U. Anselmi-Tamburini, J.N. Woolman, Z.A. Munir, Advanced Functional Materials 17 (2007) 3267.
[2] S.R. Casolco, J. Xu, J.E. Garay, Scripta Materialia 58 (2008) 516.
[3] D.A. Wright, J.S. Thorp, A. Aypar, H.P. Buckley, Journal of Materials Science 8 (1973) 876.
[4] B. Savioni, C. Ballesteros, J.E. Munoz Santiuste, R. Gonzalez, Y. Chen, Physical Review B 57 (1998) 13439.
[5] M. Niemz, Laser-Tissue Interactions Fundamentals and Applications, second revised ed., Springer, 2002, p. 38.
[6] R. Apetz, M.P.B. van Bruggen, Journal of American Ceramic Society 86 (2003) 480.
[7] D.G. Brandon, B. Ralph, S. Ranganathan, M.S. Wald, Acta Metallurgica 12 (1964) 813.
[8] M.F. Ashby, F. Spaepen, S. Williams, Acta Metallurgica 26 (1978) 1647.
[9] X. Guo, Solid State Ionics 99 (1997) 137.
[10] X. Guo, Solid State Ionics 96 (1997) 247.
[11] N. Shibata, F. Oba, T. Yamamoto, Y. Ikuhara, Philosophical Magazine 84 (2004) 2381.